PSFC/JA-09-19

An assessment of full wave effects on the propagation and absorption of lower hybrid waves

J. C. Wright, P. T. Bonoli, and A. E. Schmidt
C. K. Phillips and E. J. Valeo[1]
R. W. Harvey[2]
M. A. Brambilla[3]

July 2009

Plasma Science and Fusion Center
Massachusetts Institute of Technology
Cambridge MA 02139 USA

[1]Princeton Plasma Physics Laboratory
[2]Comp-X Del Mar, CA 92014
[3]Max-Planck-Institut fur Plasmaphysik, Euratom Association,
Boltzmannstrasse 2, D-85748 Garching bei Munchen, Germany

This work was supported by the U.S. Department of Energy, Grant No. DE-FCO2-01ER54648.Reproduction, translation, publication, use and disposal, in whole or in part, by or for the United States government is permitted.

An assessment of full wave effects on the propagation and absorption of lower hybrid waves[a]

J. C. Wright,[b] P. T. Bonoli, and A. E. Schmidt
Massachusetts Institute of Technology, Plasma Science and Fusion Center, Cambridge, Massachusetts 02139

C. K. Phillips and E. J. Valeo
Princeton Plasma Physics Laboratory, Princeton, New Jersey 08543

R. W. Harvey
Comp-X Del Mar, CA 92014

M. A. Brambilla
Max-Planck-Institut für Plasmaphysik, Euratom Association, Boltzmannstrasse 2, D-85748 Garching bei München, Germany

(Dated: June 12, 2009)

Lower hybrid (LH) waves ($\Omega_{\rm ci} \ll \omega \ll \Omega_{\rm ce}$, where $\Omega_{\rm i,e} \equiv Z_{\rm i,e}eB/m_{\rm i,e}c$) have the attractive property of damping strongly via electron Landau resonance on relatively fast tail electrons and consequently are well-suited to driving current. Established modeling techniques use WKB expansions with self-consistent non-Maxwellian distributions. Higher order WKB expansions have shown some effects on the parallel wavenumber evolution and consequently on the damping due to diffraction [G. Pereverzev, Nucl. Fusion **32**, 1091 (1991)] . A massively parallel version of the TORIC full wave electromagnetic field solver valid in the LH range of frequencies has been developed [J. C. Wright, et al., Comm. in Comput. Physics **4**, 545 (2008)] and coupled to an electron Fokker–Planck solver CQL3D [R. W. Harvey and M. G. McCoy, in Proc. of the IAEA Tech. Committee Meeting (Montreal,1992), IAEA Institute of Physics Publishing; USDOC/NTIS Doc. DE93002962, Vienna, 1993 , pp. 489-526.] in order to self-consistently evolve non-thermal electron distributions characteristic of LH current drive experiments in devices such as Alcator C-Mod and ITER ($B_0 \approx$5 T, $n_{e0} \approx 1\times10^{20}$ m^{-3}). These simulations represent the first ever self-consistent simulations of LHCD utilizing both a full wave and Fokker–Planck calculation in toroidal geometry.

I. INTRODUCTION

Lower hybrid (LH) waves have the attractive property of damping strongly via electron Landau resonance on relatively fast tail electrons at 2.5 v_{te}, where $v_{te} = (2T_e/m_e)^{1/2}$ is the electron thermal speed. Consequently these waves are well-suited to off-axis (r/a>0.60) current profile control in reactor grade plasmas with high electron temperature. It is therefore important to develop a predictive capability in this area. Advanced LH simulation codes treat wave propagation in the geometrical optics limit using toroidal ray tracing which is known to neglect important effects on the wave spectrum due to focusing and diffraction[1]. There are additional difficulties in uniquely determining the initial conditions of the rays by matching to the boundary values at an antenna or waveguide. In order to accurately assess these effects we have developed a parallel version of the TORIC full wave electromagnetic field solver valid in the LH range of frequencies with a non-Maxwellian electron dielectric response[2,3]. We observe diffractional broadening of the waves resulting in broader power deposition as compared to ray tracing. The full wave treatment described in this paper calculates the electric field amplitudes and phases directly, permitting direct application of the boundary fields from launchers in the simulation and avoids the asymptotic approximations employed in paraxial beam tracing algorithms[4] or approximations in size or geometry, or expansions in small parameters[5–7].

We find that retaining full wave effects due to diffraction and focusing has an effect on the spectral and spatial width of wave absorption. Diffraction occurs at caustic surfaces and in resonance cones resulting in an upshift of the parallel wavenumber which in turn affects the location of power deposition. By incorporating a Fokker–Planck code for self-consistent treatment of the electron distribution we account for the non-Maxwellian electron distribution that develops during LH current drive. We will compare full wave and ray tracing predictions for low and high single pass damping regimes.

In the LH range of frequencies, defined by $\Omega_{\rm ci} \ll \omega \ll \Omega_{\rm ce}$, where $\Omega_{\rm i,e} \equiv qB/m_{\rm i,e}c$ are the electron and ion cyclotron

---

[a]Paper VI 2 00003, Bull. Am. Phys. Soc. **53**, 14 (2008).
[b]Invited speaker. Electronic mail: jcwright@mit.edu

gyration frequencies in a magnetic field of strength B, plasma waves are nearly electrostatic and have very short wavelengths relative to equilibrium scale lengths. The waves are thus good candidates for a WKB approach such as ray tracing which has been the solution method of choice. However there are several known deficiencies with this approach. Lower hybrid waves are weakly damped and undergo multiple reflections from the low density cutoff at the edge of the plasma. The rays also propagate along characteristics of the electrostatic wave equation known as resonance cones that tend to become narrow and even singular at turning points forming caustics when they encircle the axis. Extended ray tracing techniques such as the Maslov method popular in seismology[8] and the wave-kinetic method[9] are valid at the caustic surfaces; but because the LH cutoffs in tokamak plasmas occur in the plasma edge where the gradients are very large, they violate the WKB approximation where the plasma is changing on the same scale as the wavelength[10].

A full wave approach that solves the Maxwell-Vlasov system directly will not be subject to these restrictions, and it will retain other physical processes that may be important to the propagation and damping of the waves. In this paper we investigate the importance of full wave effects in lower hybrid propagation using an adapted version of the TORIC code[11]. The `TORIC-LH`[3] version has been modified to solve for the fast and slow branches of the lower hybrid wave at frequencies above the lower hybrid frequency. We believe these results demonstrate the first combined full wave - Fokker–Planck calculations of LH waves in toroidal geometry of a full scale tokamak without the above approximations.

II. LOWER HYBRID PHYSICS REVIEW

Lower hybrid current drive experiments typically operate above $2\times\omega_{\rm LH}$ to avoid parametric decay instabilities[12,13]. In the lower hybrid frequency range which we take to be defined as $\Omega_{\rm ci} \ll \omega_{\rm LH} \ll \Omega_{\rm ce}$ and $\omega_{\rm LH} \equiv 1/\sqrt{1/\omega_{\rm pi}^2 + 1/|\Omega_{\rm ci}\Omega_{\rm ce}|}$, the ions are unmagnetized, that is their gyration frequency is slow compared to the wave frequency while the electrons remain strongly magnetized and the finite Larmor radius (ρ_e) approximation ($(k_\perp\rho_e)^2 \ll 1$) holds because the electron Larmor radius is much smaller that the perpendicular wavelength.

Three branches of waves are supported at this frequency: the ion plasma wave which propagates only near $\omega_{\rm LH}$ through mode conversion, the electromagnetic fast wave branch and the electrostatic branch with a slow phase velocity. The two propagating modes are described by a bi-quadratic dispersion relation[14] that determines a perpendicular wavelength and an accessibility criterion on the parallel index of refraction, $n_{\rm acc} \equiv \omega_{\rm pe}/\Omega_{\rm ce} + S$, where S is the perpendicular plasma dielectric[15] and is approximately unity in LHRF. It is the last of these that is typically referred to when speaking of lower hybrid waves in experiments. For typical Alcator C-Mod parameters of central magnetic field strength, $B_0 \approx 5T$, central electron number density, $n_{e0} \approx 7\times10^{19}{\rm m}^{-3}$, and wave frequency of 4.6 GHz, the perpendicular wavelength is about 1mm compared to $\rho_e \approx 0.1$mm and $n_{\rm acc} \approx 1.2$.

Quasilinear calculations have shown[14] that damping of the LH waves begins at a phase velocity of $\omega/k_\parallel v_{\rm te} = 2.5$ where $v_{\rm te} = \sqrt{2T_e/m_e}$ which can be restated as $n_\parallel = 5.7/\sqrt{T_e[keV]}$. Current drive efficiency scales[16] as $n_e/n_\parallel^2$ thus the accessibility limit sets the maximum current drive efficiency. Therefore, if the electron temperature is not sufficiency high ($T_e[keV] > 30/n_\parallel^2$), the most efficient current drive scenarios will be in a weak single pass absorption regime. The difference between the launched $n_\parallel$ which tends to be just above the accessibility limit, and the slower wave velocity (higher $n_\parallel$) at which damping occurs is known as the spectral gap[17]. The full wave approach suggests a new mechanism for bridging this gap, especially in devices where toroidicity is insufficient to provide geometric upshift of $n_\parallel$.

III. THE RAY TRACING APPROACH

Because of the short wavelength of LH waves relative to the system size and equilibrium gradients, an asymptotic approach to the problem is possible. In the frequency domain, the Maxwell-Boltzmann system can be expressed as a Helmholtz equation as in Eq. (1)

$$\nabla\times\nabla\times\mathbf{E} = \frac{\omega^2}{c^2}\left\{\mathbf{E} + \frac{4\pi i}{\omega}\mathbf{J}\right\}. \tag{1}$$

Codes such as `GENRAY`[18] and `ACCOME`[20] have implemented this WKB approach. Equation 2 shows the Hamiltonian ray tracing system[14] that results from the first order WKB expansion in kL of Eq. (1), where L is the scale length of the

plasma and k is the wavenumber.. The system

$$\frac{d\mathbf{x}}{dt} = -\frac{\partial D/\partial \mathbf{k}}{\partial D/\partial \omega} \tag{2}$$

$$\frac{d\mathbf{k}}{dt} = +\frac{\partial D/\partial \mathbf{x}}{\partial D/\partial \omega} \tag{3}$$

$$\frac{dP}{dt} = -2\gamma P \tag{4}$$

determines the evolution of the wavenumber and its trajectory in configuration space. These characteristics of the Hamiltonian, D, which is the dispersion function of the waves, produce rays that display certain features as shown in Fig. 1. In Equation 4, the power on each ray is represented by P and γ is the damping rate determined by the imaginary part of D. We have omitted terms representing convergence and divergence of rays (see e.g. Eqns.(6,B3) in Ram[21]) in the power evolution equation. They are formally part of the amplitude evolution, but in practice are not used both because these effects are believed to be small and because of the difficulty in initializing the second order derivatives involved.

Ray trajectories tend to display a confluence known as a caustic where individual rays converge [see Fig. 1]. At these points, a component of the wavenumber vanishes, violating the conditions for the WKB expansion. This problem can be resolved by suitable rotation in the six dimensional space of the ray equations[8], but diffraction effects that become important there are not resolved[22]. Modified WKB techniques that still follow ray trajectories but account for diffractional spreading can capture this effect[4,23]. Higher order WKB techniques that include the evolution of the amplitude can be used to calculate the electric field directly and avoid the ambiguity of which ray damps first and account for enhanced damping in caustic regions. Reflections at the cutoffs at the plasma edge where $\omega = \omega_{\rm pe}$ cannot be properly treated by WKB techniques because of the sharp gradients in the dielectric there although the rapid variation in the radial wavenumber through zero may again be treated by the Maslov technique as at caustics. Ray tracing solutions also show a high sensitivity to the plasma profiles in the edge region. This can only be avoided in high single pass absorption cases where the rays do not return to the plasma edge.

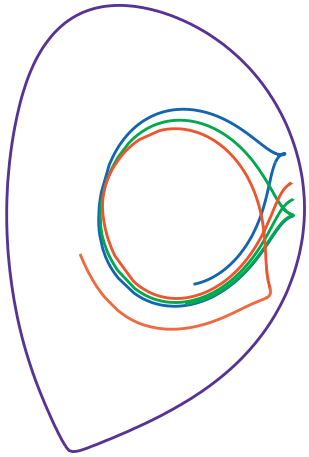

FIG. 1: (Color online) Ray tracing shows evidence of focusing at caustic surfaces shown where the three rays converge on the left part of the figure that can be treated using full wave or advanced ray tracing methods. Reflections at the cutoffs near the boundary are not properly treated by WKB techniques.

The treatment of reflections and scattering from the plasma edge is a primary concern. In reflectometry, effects from reflections off curved cutoffs were found to play an important role in the measured spectrum[24]. When waves of finite extent reflect from a curved boundary or cutoff, side bands are generated which generate new wavelengths. This scattering can then affect where the LH waves are absorbed because of the relation between absorbed $n_{\|}$ and the local electron temperature.

IV. THE FULL WAVE APPROACH

Instead of an asymptotic approach to Eq. (1), we can solve the system in Eq. (5) directly. The full wave equation is given by

$$\nabla \times \nabla \times \mathbf{E} = \frac{\omega^2}{c^2}\left\{\mathbf{E} + \frac{4\pi i}{\omega}\left(\mathbf{J}^{\mathrm{P}} + \mathbf{J}^{\mathrm{A}}\right)\right\} \tag{5a}$$

$$\mathbf{E}(\mathbf{x}) = \sum_m \mathbf{E}_m(r)\exp\left(im\theta + in\phi\right) \tag{5b}$$

$$k_\parallel = (m\mathbf{B}\cdot\nabla\theta + n_\phi \mathbf{B}\cdot\nabla\phi)/B \tag{5c}$$

$$\mathbf{J}^{\mathrm{P}}_m(r) = \sum_m \overleftrightarrow{\sigma}_c\left(k^m_\parallel, r\right)\cdot\mathbf{E}_m(r) \tag{5d}$$

where Eq. (5a) is solved by a variational technique[25] that results in a block tri-diagonal stiffness matrix. The electric field as expressed in the basis given in Eq. (5b) has the advantage of providing an algebraic expression for the parallel wavenumber in Eq. (5c) and of the plasma dielectric, $\overleftrightarrow{\sigma}_c$ needed to determine the plasma current response to the radio frequency waves as given in Eq. 5d. The radial dependence is represented by finite elements using cubic Hermite polynomials as basis functions. The plasma dielectric is a function of the magnetic equilibrium and the electron and ion distribution functions. `TORIC-LH` uses a non-Maxwellian electron distribution[26] that is analytically specified or is calculated by the Fokker–Planck code, CQL3D[19].

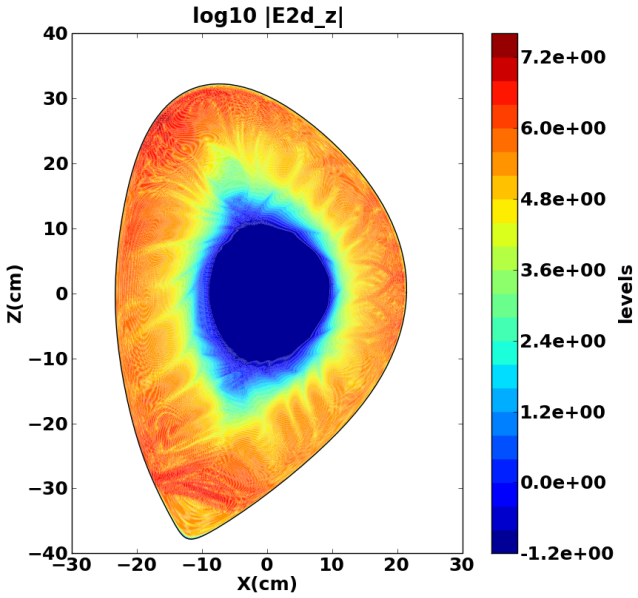

FIG. 2: Demonstration of numerical mode caused by electron FLR terms. Full wave calculation of lower hybrid waves in Alcator C-Mod at electron density of $7\times10^{19}\mathrm{m}^{-3}$ using a Maxwellian dielectric response. The field at the waveguide mouth is set at 1 V/m. A single 5cm waveguide on the right side midplane is used. The electric field component parallel to the equilibrium magnetic field is plotted. Parameters used are: f=4.6 GHz, $n_{\parallel 0}$=-1.55, N_m=1023, N_r=680, $T_e(0)$=2.3 keV, B(0)=5.4 T.

The dielectric expression used in Eq. (5d) has special considerations in the LHRF. The finite Larmor radius (FLR) contributions to $\overleftrightarrow{\sigma}_c$ are very small in this frequency range. In particular in the LHRF, the electron FLR term, $\mathbf{J}^{(2)}_e$ in Eq. (6), is proportional to the electron plasma beta, β_e, and the ion FLR term, σ, is proportional to the total plasma beta, β. Complete expressions are given in work by Brambilla[11]. In previous work[3], we discussed the need to eliminate σ, which not only is very small, but is also responsible for coupling to the evanescent (for $\omega > 2\omega_{\mathrm{LH}}$) ion plasma mode. In this paper we show in Fig. 2, that the electron FLR terms can cause a numerical mode to dominate the solution. If we include these terms in the dielectric tensor, $\overleftrightarrow{\sigma}_c$, we get the expression:

$$\overleftrightarrow{\sigma}_c\cdot\mathbf{E} = S\,\mathbf{E}_\perp + \mathrm{i}D\,(\mathbf{b}\times\mathbf{E}_\perp) + P\,E_\parallel\mathbf{b} + \nabla_\perp(\sigma\nabla_\perp\cdot\mathbf{E}) + \frac{4\pi i}{\omega}\mathbf{J}^{(2)}_e. \tag{6}$$

The terms in $\mathbf{J}_e^{(2)}$ are those responsible for transit time magnetic pumping (TTMP) and the cross term between TTMP and Landau damping (LD). They are proportional to $k_\perp^2$ and $k_\perp$ respectively, or in the full wave formulation, $\nabla_\perp$. Though these terms are negligibly small compared to the cold plasma and zero electron FLR terms, they were kept because they contribute to the electron dielectric to the zeroth order in $\Omega_{\rm ce}$ along with the Stix parallel dielectric term, P. Careful parameter scans in density and resolution indicated that the terms in $\mathbf{J}_e^{(2)}$ introduce spurious numerical modes. In the case of Fig. 2 the fields are restricted to an outer region ($r/a > 0.7$) and have an amplitude many orders of magnitude larger than the imposed field. This was thought to be caused by diffraction from the many reflections in this multi-pass low absorption scenario but in fact is entirely a consequence of how the FLR expansion is truncated. Similar effects have been observed in the ion cyclotron region[27,28], where it was noted that care must be taken to ensure terms in $k_\perp$ in different dielectric coefficients are kept consistently for certain cancellations that preserve the positive definite nature of the RF power absorption to occur.

In Fig. 3 the result of a full wave calculation in a weak single pass regime is shown with the omission of $\mathbf{J}_e^{(2)}$. In this figure, and the cases that follow, the LH antenna is represented by four 5.5 cm high waveguides 0.5 cm apart on the right side midplane with each guide launching a $\rm TE_{01}$ mode that couple only an electric field component parallel to the equilibrium magnetic field. A single toroidal mode is used representing the peak of the launched spectrum, $n_{\|0}$. Throughout this paper, we use the convention that the sign of the parallel index is with respect to the direction of the equilibrium magnetic field. Current has the opposite direction as the driven electron motion because of their negative charge and electrons are driven in the same direction as the sign of $n_{\|0}$. Simulations use parameters from Alcator C-Mod which is generally operated in a co-current configuration, and so current drive phasing of the waveguides has a negative value for $n_{\|0}$. The spectral width of the waveguide spectrum is determined by the poloidal spectrum from the finite height of the guides. This provides a realistic representation of the waveguide geometry and its poloidal spectrum. The contrast with Fig. 2 is clear: the wave fields now penetrate to the core and fill the volume of the torus as a consequence of the weak single pass damping. In the succeeding sections we will consider questions of spectral convergence, power deposition, and the effect of non-thermal features in the multi-pass case.

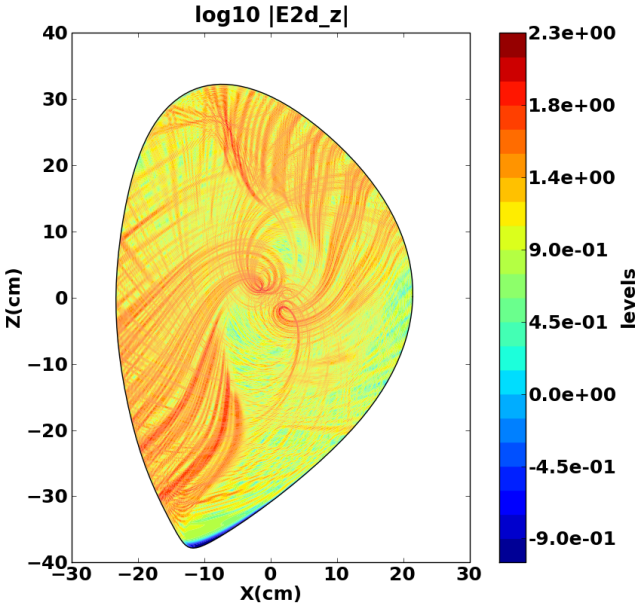

FIG. 3: Full wave calculation of lower hybrid waves in Alcator C-Mod at electron density of $7 \times 10^{19}\mathrm{m}^{-3}$ using a Maxwellian dielectric response. The magnitude of the complex electric field component parallel to the equilibrium magnetic field is plotted on a logarithmic scale. The field at the waveguide mouth is set at 1 V/m. Parameters used are: f=4.6 GHz, $n_{\|0}$=-1.55, N_m=1023, N_r=980, $T_e(0)$=2.3 keV, B(0)=5.4 T.

V. FULL WAVE EFFECTS AND NON-THERMAL ELECTRONS

Calculation of propagation with the full wave approach shows striking similarities and some differences from the ray tracing approach. The wave fields reveal beam like patterns such as in Fig. 3 that follow the classic resonance cone trajectories[29] and are also seen in the paths of rays from WKB codes. Figure 4 compares the radial power deposition in the two approaches. Despite the difference in the approaches, nearly identical power deposition profiles are found.

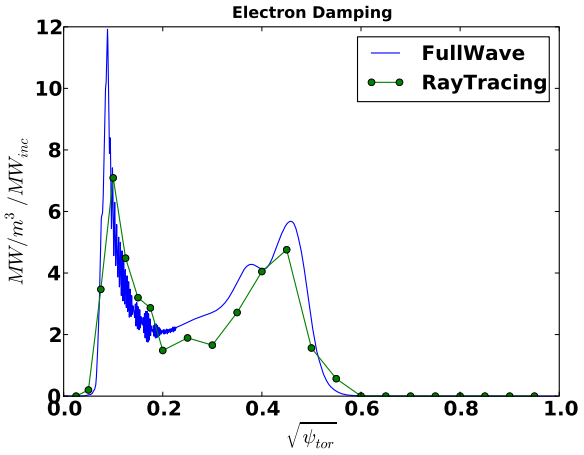

FIG. 4: (Color online) Comparison of radial location of power deposition profiles between ray tracing and full wave calculations for the Alcator C-Mod case at a density of $n_e(0) = 7{\times}10^{19}\mathrm{m}^{-3}, n_\parallel = -1.55, N_m = 1023, N_r = 980, T_e(0) = 2.3keV, B(0) = 5.4T$. Power deposition profiles for the ray tracing were interpolated onto 23 flux surfaces.

We expect some enhanced spectral broadening and acceleration of the filling of the spectral gap in the presence of diffraction in the full wave solver. The primary sources of this diffraction are caustic surfaces and scattering during reflections from the plasma cutoff. However, in the case of damping on a Maxwellian, we see no indication of this in the power deposition. That is, the damping profiles from the full wave do not show a significant difference from those of ray tracing which lacks these effects.

We can isolate any effect of reflections by adjusting the parameters to create a single pass absorption case. Increasing the magnitude $n_{\parallel 0}$ to -3.6 while keeping all other parameters constant achieves this. In Fig. 5, the fields are no longer space filling. The short paths no longer return to the launcher interfering and obscuring the four launched waves which are now clearly visible. The wave trajectories focus as they approach the center of the plasma and spread again via diffraction and refraction as they leave and undergo a radial reflection from the cut off at the plasma edge, before damping. The contours of the parallel electric field for the full wave solutions show the formation of a caustic surface near the center and have lower amplitude fields throughout. This is to be contrasted with Fig. 3, where the field amplitude is over an order of magnitude larger in weak absorption because of the cavity effect, in which the source amplitude is magnified if damping is weak in the cavity. This effect does not normally manifest in experiment, rather, the electron distribution function evolves to provide significant damping. We have also shown in Fig. 5 a comparison of the full-wave radial deposition profiles for the strong absorption case with the ray tracing prediction. Note the profiles agree qualitatively in shape from $0.35 < \mathrm{r/a} < 0.8$.

To self-consistently determine the electron distribution and the damping, we iterate between the full wave `TORIC` code and the Fokker–Planck CQL3D code. The coupling between the two codes takes place through the RF induced quasilinear diffusion,D_{ql}, in velocity space in CQL3D and the use of a non-Maxwellian parallel dielectric in `TORIC`. The formulation of the parallel diffusion coefficient, $D_\parallel$, from Eqns. (37-39) in work by Harvey and McCoy[19] which is a relativistic generalization of the Kennel and Engelmann[30] derivation is given by

$$D_\parallel = \frac{q^2}{2m^2}\pi\delta\left(\omega - k_\parallel v_\parallel\right)\left|u_\parallel E_\parallel\right|^2\left(\frac{k_\parallel}{\omega\gamma}\right)^2, \tag{7}$$

in which we have kept only the zeroth order electron FLR terms and γ is the relativistic Lorentz factor, δ is the usual delta function resonance, and $u = p/m$ is the relativistic particle momentum per rest mass. This expression is evaluated and bounce averaged assuming zero banana width electrons in a post-processing mode of `TORIC`. It is then mapped onto the polar velocity space mesh and stored in a format used by CQL3D. CQL3D uses this diffusion coefficient scaled to couple the desired amount of power. This is necessary because the full wave code is linear and the amount of power coupled by the waveguide depends on the plasma loading as well as the electric field specified at the guide. The scale factor needs only to be adjusted at the beginning of the iteration. The loop is closed by the use of the CQL3D generated electron distribution function,$f_e(\mathbf{v})$, in the next run `TORIC`. Because LH interacts with electrons at parallel speeds greater the 2.5 times the thermal velocity, only the anti-Hermitian part of the parallel dielectric is affected. Therefore, in Eq. (6) only damping in P is modified and it is proportional to the parallel velocity space derivative of $f_e(\mathbf{v})$[15]. The two codes are iterated in this coupled fashion until the power deposition no longer

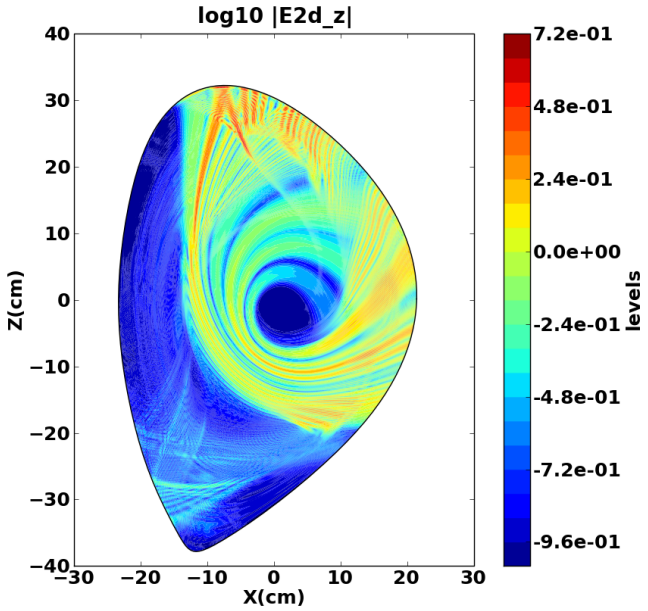

FIG. 5: Strong absorption case. Full wave calculation of lower hybrid waves in Alcator C-Mod at electron density of $7\times10^{19}\mathrm{m}^{-3}$ using a Maxwellian dielectric response. $n_{\|0}=-3.6, N_m=1023, N_r=980, T_e(0)=2.3keV, B(0)=5.4T$

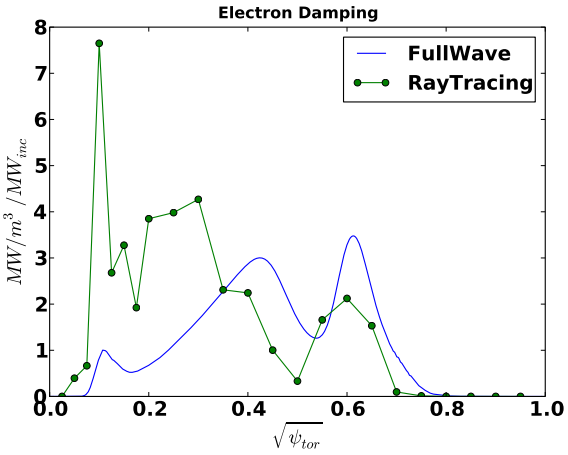

FIG. 6: (Color online) Strong absorption. Comparison of radial location of power deposition profiles between ray tracing and full wave calculations for the Alcator C-Mod case at a density of $n_e(0)=7\times10^{19}\mathrm{m}^{-3}, n_\|=-3.6, N_m=1023, N_r=980, T_e(0)=2.3keV, B(0)=5.4T$

changes and agrees between the two codes.

By observing the evolution of non-Maxwellian features in the electron distribution we can see direct evidence of the spectral broadening. For the low single pass absorption case, we have used the electric fields from the full wave solution shown in Fig. 7 to formulate the RF quasilinear diffusion coefficient. This was then employed in the Fokker–Planck code CQL3D to evolve the electron distribution function. Compared to Fig. 3, the electric fields are less intense and have penetrated further into the plasma. In Fig. 8, we see the formation of a quasilinear plateau clearly at a pitch angle of $\theta=0$ at a flux surface of $r/a\sim0.5$ located in the region of power absorption in the weak single pass case. The plateau extends in a range of parallel velocities corresponding to $n_\|=[1.4,5]$([1.1,0.2] on the relativistic velocity scale in the plot) demonstrating clear evidence of downshift of the phase velocity. from the launched $n_\|$ of -1.55 to fill the spectral gap. Up-shifting is also apparent as the injected phase velocity in the figure corresponds to a value of $\gamma v/c=0.71$.

The damping from the quasilinear modifications of $f_e(\mathbf{v})$ have a strong effect on the convergence of the spectral

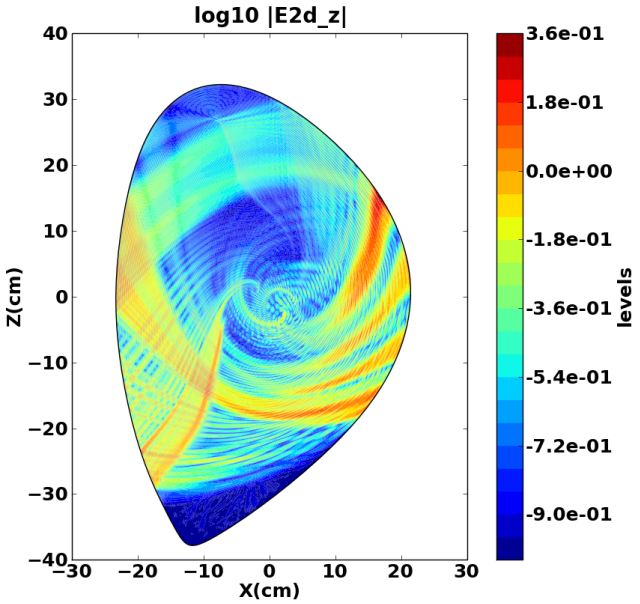

FIG. 7: Full wave calculation of lower hybrid waves in Alcator C-Mod at electron density of $7 \times 10^{19}\mathrm{m}^{-3}$ using a self-consistent non-Maxwellian dielectric response achieved after four iterations. The electric field component parallel to the equilibrium magnetic field is shown. Parameters used are $n_\parallel = -1.55, N_m = 1023, N_r = 980, T_e(0) = 2.3keV, B(0) = 5.4T$.

expansion. In Fig. 9, we show the power spectrum of the solution from Fig. 7. The power spectrum demonstrates strong convergence even at outer flux surfaces. The energy in the largest magnitude poloidal modes is orders of magnitude lower than the peaks in the spectrum at each flux surface. We also observe the asymmetric nature of the spectrum. For the value of $n_{\parallel 0}$, positive poloidal mode numbers decrease the magnitude of the local value of $n_\parallel$ bring the value closer to the accessibility limit. Once reached, we see the sharp and continuous exponential drop in amplitude. For negative poloidal modes, the phase velocity is shifted towards the bulk electrons where damping is strong and we see the more structured decrease in the spectrum. The power spectrum for the first field solution with Maxwellian damping (Fig. 3) is only converged to about a radius of $r/a \approx 0.6$ as the damping reduces with temperature at outer flux surfaces and the contribution of the poloidal mode number to $n_\parallel$ is reduced by the safety factor at larger radii limiting the amount of downshift in the phase velocity possible. Larger numbers of modes $N_m = 2047$ will converge the Maxwellian case and result in more growth of the fields in the plasma due to the previously discussed cavity effect. The meaning of such convergence is questionable as well since the distribution function does not remain Maxwellian and after even the first iteration, the established quasilinear plateau is sufficient to converge the spectrum at $N_m = 1023$ modes. In general, the stronger the damping, the faster the convergence and the fewer modes required for convergence, subject to resolving the scale lengths of the launch modes in the given geometry.

VI. CONCLUSIONS

We have shown calculations for the first time of LH waves in toroidal geometry in a present day sized tokamak. Realistic general geometry and non-Maxwellian electrons were used. These simulations predict similar power absorption locations for the waves as traditional ray tracing approaches. Scattering at cutoffs in the edge of the plasma has been identified as an important mechanism in lower hybrid wave diffraction and was shown to affect the power deposition location. Scattering manifests itself in low single pass absorption regimes that are common in present day tokamaks with modest electron temperature where LH RF power is used with low parallel index of refraction to maximize the driven current. Full wave simulations are necessary to accurately predict the location of the current driven in these devices. In higher temperature ($T_e[keV] > 30/n_\parallel^2$) devices such as ITER there is high single pass absorption and scattering effects may play a minimal role. In the future we plan to compare the predicted hard x-ray signals based on the full wave-Fokker Planck calculation with the hard x-ray spectra measured in the Alcator C-Mod experiment and with spectra simulated based on a ray tracing - Fokker Planck treatment[31]. These types of comparisons should help to validate the ray tracing and full-wave approaches as well as providing insights into how important full-wave effects are for understanding the experiment.

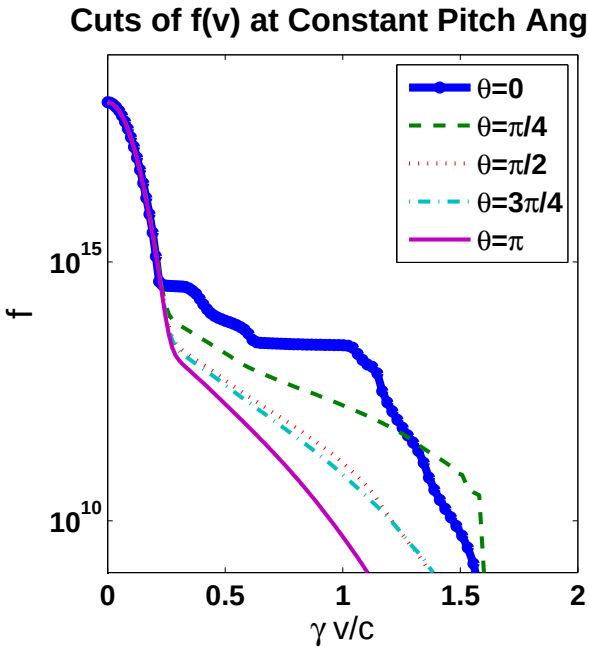

FIG. 8: (Color online) Electron distribution response to the LH waves' quasilinear flux generated from the fields in Fig. 7. Plots of the distribution function versus relativistic velocity measure for several different pitch angles, θ, at a flux surface of $r/a \sim 0.50$ in the multi-pass case. Parameters are the same as listed in Fig. 7. γ is the relativistic Lorentz factor. 650 kW of power were coupled in this case.

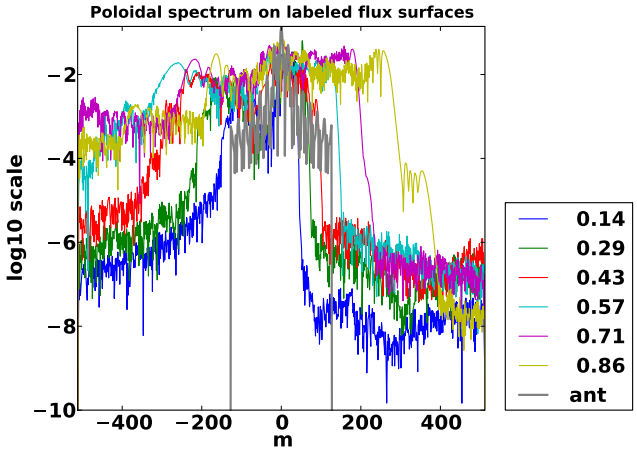

FIG. 9: (Color online) The poloidal power spectrum plotted for several flux surfaces and the waveguide surface for the parameters in Fig. 7.

ACKNOWLEDGMENTS

We would like to thank Professor Ronald Parker, Professor Miklos Porkolab, and Greg Wallace for many enlightening discussions during the course of this work.

This research was sponsored by the DOE Wave–Particle SciDAC (Scientific Discovery through Advanced Computing) Contract No. DE-FC02-01ER54648.

[1] G. V. Pereverzev, Nucl. Fusion **32**, 1091 (1992).
[2] E. J. Valeo, C. K. Phillips, P. T. Bonoli, and J. C. Wright, in *17th Topical Conference on Radio Frequency Power in Plasmas*, edited by P. Ryan, and D. Rasmussen American Institute of Physics, New York, 2007 , No. 933, p. 297.
[3] J. C. Wright, E. J. Valeo, C. K. Phillips, P. T. Bonoli, and M. Brambilla, Commun. Comput. Phys. **4**, 545 (2008).
[4] N. Bertelli, G. V. Pereverzev, and E. Poli, in *34th EPS Plasma Physics Conference* 2007 , editted by Pawel Gasior and Jerzy Wolowski (European Physical Society, 2007) vol. 31F of *Europhysics conference abstracts*, URL `http://epsppd.epfl.ch/Warsaw/start.htm`.
[5] J. J. Schuss, Physics of Fluids **28**, 1779 (1985).
[6] Y. Peysson, E. Sébelin, X. Litaudon, D. M. J.-C. Miellou, M. M. Shoucri *et al.*, Nucl. Fusion **38**, 939 (1998).
[7] M. A. Irzak, in *30th EPS Conference on Contr. Fusion and Plasma Phys.*, edited by R. Koch, and S. Lebedev European Physical Society, 2003 , vol. 27A of *Europhysics conference abstracts*, p. P2.175, URL `http://epsppd.epfl.ch/StPetersburg/start.html`.
[8] C. H. Chapman, and H. Keer, Stud. Geophys. Geo. **46**, 615 (2004).
[9] K. Kupfer, D. Moreau, and X. Litaudon, Phys. Fluids B **5**, 4391:4407 (1993).
[10] M. Brambilla, and A. Cardinali, Plasma Phys. **24**, 1187 (1982).
[11] M. Brambilla, Plasma Phys. Controlled Fusion **41**, 1 (1999).
[12] M. Porkolab, Phys. Fluids **20**, 2058 (1977).
[13] M. Porkolab, IEEE Trans. Plasma Sci. **PS-12**, 107 (1984).
[14] P. Bonoli, IEEE Trans. Plasma Sci. **PS-12**, 95 (1984).
[15] T. H. Stix, *Waves in Plasmas* American Institute of Physics, New York, 1992 .
[16] N. J. Fisch, Phys. Rev. Lett. **41**, 873 (1978).
[17] P. T. Bonoli, and R. C. Englade, Phys. Fluids **29**, 2937 (1986).
[18] A. P. Smirnov, R. W. Harvey, and K. Kupfer, in *Bull Amer. Phys. Soc.* **39**, 1626 (1994).
[19] R. W. Harvey, and M. G. McCoy, in *Proc. of the IAEA Tech. Committee Meeting (Montreal,1992)*, IAEA Institute of Physics Publishing; USDOC/NTIS Doc. DE93002962, Vienna, 1993 , pp. 489–526.
[20] R. S. Devoto, D. T. Blackfield, M. E. Fenstermacher, P. T. Bonoli, M. Porkolab *et al.*, Nucl. Fusion **32**, 773 (1992).
[21] A. K. Ram, and A. Bers, Phys. Fluids B **3**, 1059 (1991).
[22] J. B. Keller, J. Opt. Soc. Am. **52**, 116 (1962).
[23] P. Rodrigues, and J. P. S. Bizarro, IEEE Trans. Plasma Sci. **30**, 68 (2002).
[24] Y. Lin, R. Nazikian, J. H. Irby, and E. S. Marmar, Plasma Phys. Controlled Fusion **43**, L1 (2001).
[25] M. Brambilla, and T. Krücken, Nucl. Fusion **28**, 1813 (1988).
[26] E. J. Valeo, J. C. Wright, R. Bilato, P. T. Bonoli, M. Brambilla *et al.*, in *35th EPS Conference on Contr. Fusion and Plasma Phys.*, edited by P. Lalousis, and S. Moustaizis European Physical Society, 2008 , vol. 32D of *Europhysics conference abstracts*, p. P2.099, URL `http://epsppd.epfl.ch/Hersonissos/start.htm`.
[27] C. K. Phillips, J. R. Wilson, J. C. Hosea, R. Majeski, and D. N. Smithe, Phys. Plasmas **1**, 3905 (1994).
[28] C. Y. Wang, D. B. Batchelor, and E. F. Jaeger, Phys. Plasmas **2**, 2863 (1995).
[29] P. M. Bellan, and M. Porkolab, Phys. Plasmas **17**, 1592 (1974).
[30] C. F. Kennel, and F. Engelmann, Phys. Fluids **9**, 2377 (1966).
[31] P. T. Bonoli, A. E. Hubbard, J. Ko, R. Parker, A. E. Schmidt *et al.*, Phys. Plasmas **15**, 056117 (2008).